Study of drop coalescence and mixing in microchannel using Ghost Particle Velocimetry

Kovalchuk, N. M.; Chowdhury, J.; Schofield, Z.; Vigolo, D.; Simmons, M. J. H.

DOI:
10.1016/j.cherd.2018.01.034

Contents lists available at ScienceDirect

Chemical Engineering Research and Design

journal homepage: www.elsevier.com/locate/cherd

Study of drop coalescence and mixing in microchannel using Ghost Particle Velocimetry

N.M. Kovalchuk, J. Chowdhury, Z. Schofield, D. Vigolo, M.J.H. Simmons*

University of Birmingham, Edgbaston, Birmingham B15 2TT, UK

ARTICLE INFO

Article history:
Received 31 October 2017
Received in revised form 13 December 2017
Accepted 16 January 2018
Available online 31 January 2018

Keywords:
Microfluidics
Ghost Particle Velocimetry
Flow patterns
Coalescence kinetics
Surfactant

ABSTRACT

The coalescence of drops formed in a flow focusing microfluidic device at Reynolds number $0.1 < Re < 1$ was studied experimentally using high speed video-recording and Ghost Particle Velocimetry. It was shown that in the confined microfluidic geometry the presence of both ionic and non-ionic surfactants can facilitate drop coalescence for surfactants dissolved in either the dispersed or the continuous phase. Drop merging was accompanied by strong convection inside the drops with maximum velocity exceeding the superficial liquid velocity by one order of magnitude. Intensity of convection increased with a decrease of drop size and decreased with a decrease of interfacial tension between continuous and dispersed phase. Effect of drop size was particularly strong when the drop size exceeded 80% of the channel width due to the considerably thinner film of continuous phase separating dispersed phase from the channel wall, slower expelling of continuous phase surrounding growing neck between merging drops and therefore slower neck thickening. When merging drops of different sizes was considered, the convection was much stronger in the small drop and movement of the contents of the smaller drop towards the larger drop was observed.

1. Introduction

Droplet microfluidic systems are promising tools for chemical analysis and synthesis providing highly controllable reaction conditions, minimal advective dispersion and short diffusion distances due to small reactor size (DeMello, 2006; Seemann et al., 2012; Stone et al., 2004; Tice et al., 2003; Whitesides, 2006). Using flow devices for drop production and manipulation adds the advantages of high-throughput as drops can be generated on millisecond time scale (Casadevall i Solvas et al., 2010) and study of reaction kinetics (Song et al., 2003). Using on-chip impedance measurements taken in real time to control the droplet injection enables addition of reagents at the exact time and location within the device, i.e. at desired age of the primary drop (Axt et al., 2017).

There are two ways to introduce reagents into a drop microreactor. In one approach the streams of reagent containing solutions are injected into the continuous phase at a T or cross-junction where drops containing all necessary reagents are formed (Bringer et al., 2004; DeMello, 2006; Song et al., 2003; Tice et al., 2003). Winding (serpentine) output channels are used in this case to improve convective premixing of regents by generating chaotic advection inside the drops. Convective premixing decreases further the striation length over which diffusion mixing takes place and therefore further decreases the diffusion mixing time.

In the second approach, drops containing different reagents are formed separately and then deliberately coalesced in the output channel. Drop coalescence in this case is a trigger for reaction to start. This approach was used by Frenz et al. (2008) for synthesis of magnetic particles of iron oxide. They noted that using coalescing drop is preferable for aggressive or fast reactions which form precipitates. Other advantages of the drop coalescence method are that the moment at which the reaction starts is precisely set and there is additional convective mixing caused by coalescence. There are a lot of active and passive methods proposed for controlled drop coalescence (Bremond and Bibette, 2012; Frenz et al.,

* *Corresponding author.*
E-mail address: n.kovalchuk@bham.ac.uk (N.M. Kovalchuk).
https://doi.org/10.1016/j.cherd.2018.01.034

2008; Gu et al., 2011; Lee et al., 2016; Nurdin et al., 2016). Winding channels can be used also in drop coalescence approach to improve the mixing. It was for example proposed by Sarrazin et al. (2007) that the optimal mixing is achieved at coalescence of the drops aligned in the straight channel along the channel axis with further movement of coalesced drop through a 45° bended channel.

Drops moving along the channel undergo shear stresses due to the relative velocity of the continuous phase which is subjected to the no slip condition on the channel wall. These stresses result in circular motion inside the moving drop with symmetry axis parallel to the flow direction and in straight channels this coincides with the channel axis (Rhee and Burns, 2008; Sarrazin et al., 2006; Seemann et al., 2012; Pirbodaghi et al., 2015). This circular motion mixes the contents of two coalescing drops if they are aligned in the flow direction, whereas no mixing is expected for the content of drops moving side by side with coalescence axis being perpendicular to the flow direction. Winding channels accelerate mixing in the last case. Obviously, the thinner is the film of continuous phase the faster is the recirculatory mixing.

This study is focused on the coalescence of drops aligned along the flow direction taking advantage of the recirculatory mixing. Drops containing different reagents can be produced and coalesced using for example design of microfluidic device proposed by Hung et al. (2006) or by Frenz et al. (2008). Note, besides well studied recirculatory convection due to motion inside the channel (Rhee and Burns, 2008; Sarrazin et al., 2006; Seemann et al., 2012), drop coalescence itself causes and additional convection which can further facilitate mixing.

There are several numerical (Blanchette, 2010; Martin and Blanchette, 2015; Nowak et al., 2017) and experimental (Chinaud et al., 2016; Nowak et al., 2017; Yeh et al., 2013) studies on drop coalescence in unconfined or partially confined (drops on a substrate, Hele-Shaw cell) flow geometries. The convective patterns resulting from drop coalescence in microchannels are much less studied. Jin and Yoo (2012) studied coalescence of two drops of glycerol/water mixture in continuous phase of silicone oil in a straight and in a divergent channel. In the straight channel the drops size was different to create a difference in the drop velocities, whereas drops of similar size were studied in divergent channel, where the velocity difference was due to channel geometry. It was found by Jin and Yoo (2012) that in the reference frame related to the advanced meniscus of the front drop the rear drop penetrates the front drop without formation of noticeable vortex motion in the straight channel. In the divergent channel coalescence resulted in strong back flow and vortices formation in the front drop. To our knowledge, the effect of drop/channel size ratio and the effect of surfactant on kinetics of drop coalescence and flow fields inside the coalescing drops in micro-channels has not been previously examined and this is one of the goals of this study. Analysis of the flow inside the droplets will enable better understanding of the coalescence phenomena because kinetics of coalescence is determined by the inflow of liquid into growing neck, which, in turn, depends not only on capillary pressure difference but also on viscosities on liquid phases, their mutual motion and confinement imposed by microchannel.

Besides controlled coalescence, the delivering of monodisperse drops of prescribed size to reaction site is of crucial importance for microfluidic reactors. Therefore coalescence of drops in delivery channels has to be prevented. It is well known that surfactants are used to stabilise drops against the coalescence, including microfluidic applications (Baret, 2012). However, it was shown recently by Kovalchuk et al. (2017) that under confined conditions in micro-channels some surfactants can facilitate coalescence instead of preventing it. Therefore another goal of this study is the deeper insight into effect of surfactant on coalescence rate of drops in microchannels.

The present work illustrates the results on the formation and coalescence of water drops in a continuous oil phase, thus covering the case of micro-reactors for water soluble reagents. In particular, we will focus on (i) the effect of surfactant of drop coalescence rate, (ii) the convective flow patterns due to drop merging and (iii) the effect of surfactant and drop size on the intensity of convective motion. The flow patterns inside the merging drops are studied by Ghost Particle Velocimetry (Buzzaccaro et al., 2013; Pirbodaghi et al., 2015; Martino et al., 2016).

2. Materials and methods

The surfactants, dodecyltrimethylammonium bromide (C_{12}TAB), Across organics, 99%; sodium dodecyl sulphate (SDS), Sigma–Aldrich, ACS reagent, ≥99%; Triton X-100, Sigma–Aldrich, laboratory grade; Span 80, Sigma; as well as glycerol, Alfa Aesar, ultrapure, HPLC grade and silicone oil (SO), viscosity standard 5 cSt, Aldrich were used as purchased. Double-distilled water was produced by a water still Aquatron A 4000 D, Stuart.

The aqueous phase used in this study was 52% glycerol/48% water mixture (GW) (Physical properties of glycerine and its solutions, 1963) in order to match the refractive index of the oil phase $n = 1.403$. Matching the refractive indices of continuous and dispersed phases avoids optical distortions at the interface and enables better resolution of flow fields near the interface. C_{12}TAB is a cationic and SDS is an anionic surfactant, both soluble only in aqueous phase, Triton X-100 and Span 80 are non-ionic surfactants soluble in both aqueous and oil phase, but Triton X-100 partition is greatly in favour of aqueous phase, whereas that of Span 80 is greatly in favour of oil. Water in oil emulsions have been studied with two cases considered: surfactant present in dispersed or in continuous phase.

Experiments were performed using a Droplet Junction Chip (cross-junction), Dolomite Microfluidics, UK, made of glass with hydrophobised channels. The geometry as presented in Dolomite Product Datasheet is shown in Fig. 1. The liquids were supplied to the chip using syringe pumps Al-4000 (World Precision Instruments, UK), equipped with 10 mL syringes (BD Plastipak^{TM}) at flow rates dispersed, Q_d, and continuous, Q_c, phases in the range of 3–50 μL/min with Reynolds number being in the range $0.1 < Re < 1$, based on the superficial liquid velocity evaluated at the output channel and its hydraulic diameter, as a consequence, laminar flow regime is expected in all experiments. Note, in what follows Q_c corresponds to the flow rate in each channel supplying the continuous phase. Therefore the superficial flow rate in the output channel is $Q_o = Q_d + 2Q_c$. After any change in flow rate the system was allowed to stabilise for at least 10 min. The drops formation, movement and coalescence was monitored at 2000 fps using a high speed video-camera (Photron SA5) equipped with a Navitar, 2X F-mount objective. To enhance optical contrast methyl violet dye, Sigma–Aldrich, was dissolved in aqueous phase in concentrations 0.5–1 g/L. The presence of dye did not change

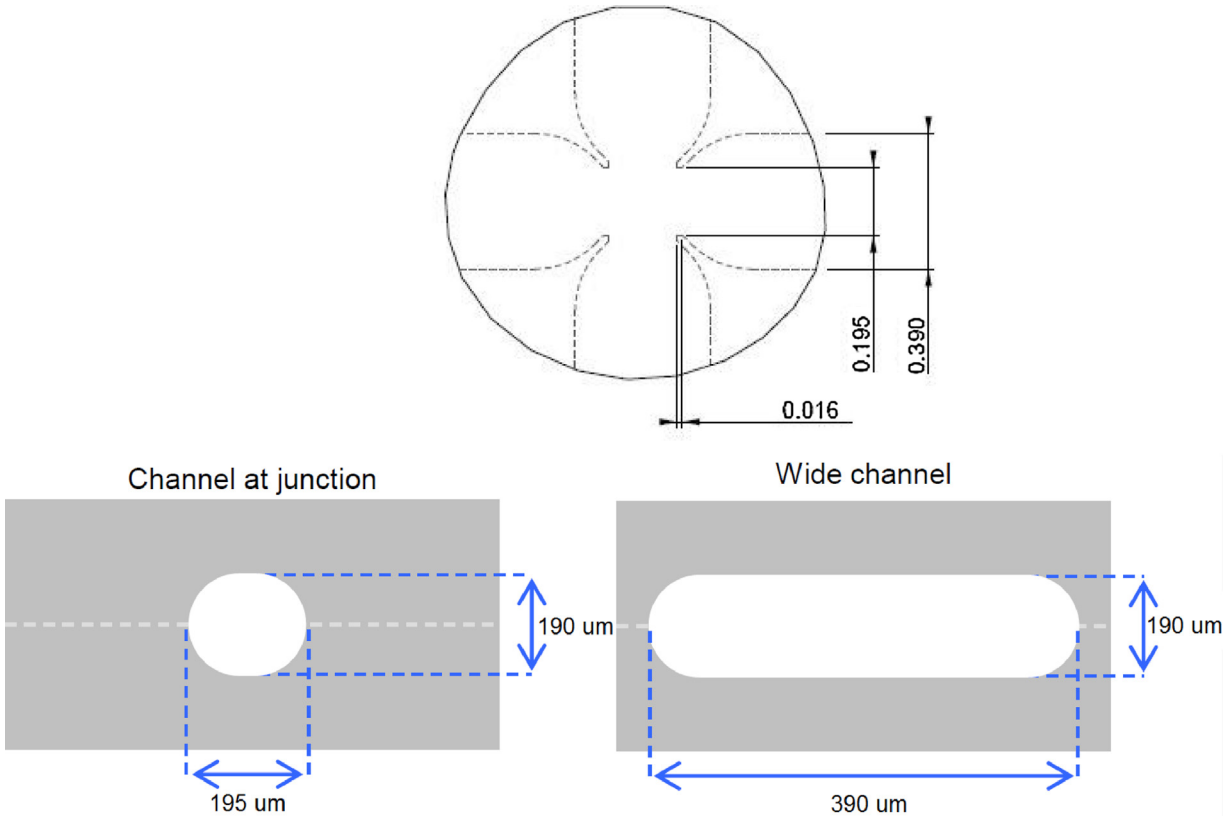

Fig. 1 – Microfluidic chip geometry.
Adapted with permission from the Dolomite Product Datasheet.

the interfacial tension between the oil and aqueous phase above the level of experimental error. Image processing was performed using ImageJ free software.

Ghost Particle Velocimetry (Buzzaccaro et al., 2013; Pirbodaghi et al., 2015; Martino et al., 2016) was used to study the flow patterns inside the drop after coalescence. This technique exploits standard white light illumination provided by an optical microscope to generate a speckle pattern used to map the flow field. The latter is originated by the light scattered by tracers smaller than the diffraction limit (i.e., about 300 nm for visible light). By reducing the numerical aperture of the condenser lens, it is in fact possible to obtain coherent illumination within a thin volume of the sample. The thickness of this volume can be approximated by $\delta_z \approx \lambda/NA_C$ where λ is the wavelength of the light used and NA_C is the numerical aperture of the condenser (typically $NA_C \approx 0.15$–0.2), which translates into a resolution of few tens of micrometres (Buzzaccaro et al., 2013). In the present work the dispersed phase was seeded with 0.2% w/v concentration of 200 nm polystyrene particles (Sigma). Experiments were performed in horizontal channel; therefore the effect of channel inclination on flow patterns was not studied.

The video-recording was performed at 10,000 fps and shutter set to 0.02 ms. The high-speed video-camera was connected to an inverted microscope (Nikon eclipse Ti-U), a 20× objective (Nikon, CFI Plan Fluor DLL) was used giving an image resolution of 1 μm/pixel. In order to better discriminate the speckle pattern signal from the background noise, the median of several frames (typically >100 frames) was subtracted to each frame (Pirbodaghi et al., 2015) using ImageJ. In this way the static contribution (mainly due to the presence of the microchannel and the droplets themselves) was removed and only the moving speckle pattern remained.

The speckle pattern analyses was then performed using PIVlab v 1.4, an open-source MATLAB toolbox (Thielicke and Stamhuis, 2014), in order to obtain the flow field. It is in fact possible to use the same algorithm used to perform flow field analyses for Particle Image Velocimetry (PIV) to analyse the speckle pattern obtained by GPV. Briefly, a cross-correlation between pairs of sequential frames detects the displacement of each region of interest (ROI) within the frame, and by knowing the frame rate of the image acquisition this can be translated into local velocity. It is important to note that a minimum number of speckles needs to be contained in each ROI in order to get sensible results. Additionally, the displacement should be smaller than the lateral size of the ROI (as a rule of thumb, typically less than 1/2 of the later size). Considering that the size of a single speckle is independent of the particle size (in far field optics), and only minimally affected by the optical elements used, practically this fixes its size to ~2 to 3 μm; the minimum size of the ROI used was about 20 × 20 pixels (and so about 20 μm × 20 μm), which is the in-plane resolution of these measurements.

The equilibrium interfacial tension was measured using a tensiometer K100 (Krüss) equipped with a Du Noüy platinum ring or Wilhelmy plate. The dynamic surface tension was measured using a maximum bubble pressure tensiometer BPA-1S (Sinterface, Germany). The viscosity was measured by a TA instruments Discovery-HR-2 rheometer in flow mode using cone and plate geometry with the angle 2° 0′ 29″ and a truncation of 55 μm.

The physical properties of the liquids used in this study are presented in Table 1 and interfacial tensions are given in Table 2.

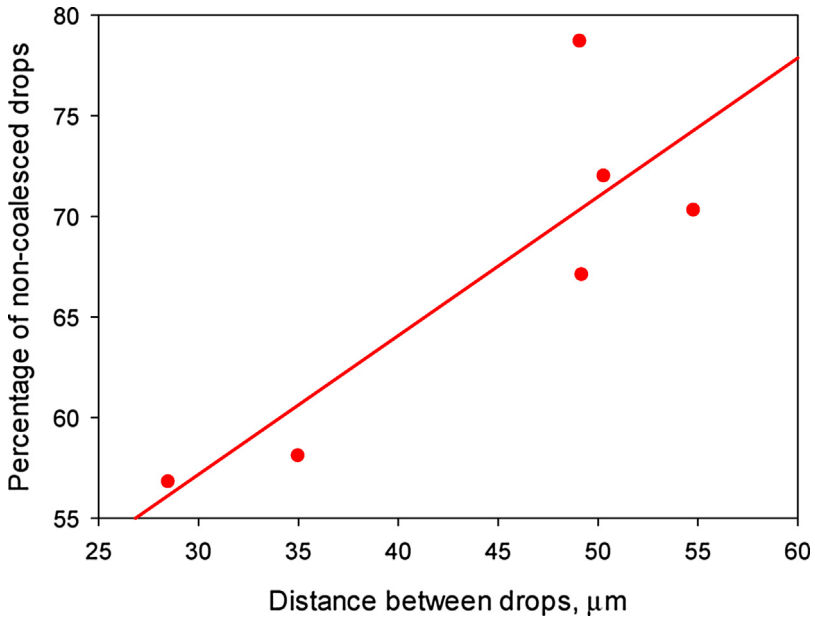

Fig. 2 – Dependence of percentage of non-coalescing drops of surface to surface distance between them. Surfactant-free system, Q_c = 10 μL/min, Q_d = 14 μL/min, observation length L = 3.4 mm.

Table 1 – Physical properties of the liquid phases.

Liquid	Density, kg/m^3	Dynamic viscosity, mPa s
Water/glycerol mixture 52:48 (w:w)	1133 ± 2	6.4 ± 0.4
Silicone oil	920	4.6

Table 2 – Equilibrium interfacial tensions of surfactant solutions.

Continuous phase	Dispersed phase	σ, mN/m
SO	GW	29
SO	GW + 50 mM SDS	10
SO	GW + 50 mM SDS	9
SO	GW + 50 mM Triton X-100	3
SO + 25 mM Span 80	GW	1

3. Results and discussion

3.1. *Effect of surfactant on the rate of drop coalescence*

It was observed in Kovalchuk et al. (2017) that aqueous drops formed in microfluidic device presented in Fig. 1 can coalesce in the straight output channel, which is an undesirable event in the production of monodisperse set of drops. It was also observed that the alkyltrimethylammonium bromide family of cationic surfactants remarkably facilitated coalescence instead of preventing it. This process revealed itself in two ways: (i) drops approach each other considerably faster in the presence of surfactant and (ii) coalescence occurs rapidly after the drops contact: the time scale of coalescence, $t < 0.5$ ms, is considerably smaller than reported in the literature. Below the effect of anionic and non-ionic surfactants on the rate of drop coalescence is considered.

The distance between drops in micro-channel can change even in the absence of forces between them, simply due to difference in the drop size. The smaller drops move faster than the larger ones because of the parabolic flow profile of the laminar flow of viscous liquid and therefore the distance between drops will decrease with time if the larger drop is followed by the smaller one and will increase with time otherwise. Coalescence was observed for drops with diameters in the plane of observation between 200 μm < D < 370 μm, smaller than the channel width, but larger than the channel height, i.e. these drops have a pancake-like shape. For the drops in this size range the scattering in the diameter values was inside 2% independently of drop size. Therefore it can be expected that there is no noticeable dependence of approach rate on drop size.

The rate of coalescence (percentage of coalesced drops) depends on the distance from the junction where the drops are formed, or, in other words, on the time two drops have to get close to each other and coalesce. Under conditions of the present study the coalescence of surfactant-free drops was observed within 3 mm of channel length at flow rates of dispersed phase $Q_d \leq 20$ μL/min and $1 \leq Q_d/Q_c \leq 2$. As a basis for comparison in coalescence rate between surfactant-laden and surfactant-free drops we have chosen the conditions Q_c = 10 μL/min, Q_d = 10 μL/min and observation length of channel L = 3 mm. If flow rates were different from the basic set, the channel length for observation was changed proportionally to ensure the constant time given for coalescence. For example for Q_c = 10 μL/min, Q_d = 14 μL/min the observation length was 3.4 mm (Table 3).

It is expected that the coalescence rate should decrease with an increase of the initial distance between the drops, Δ, because drops need more time to get together at the same approach velocity. This assumption is supported by Fig. 2, where results for different runs for surfactant-free system at Q_c = 10 μL/min, Q_d = 14 μL/min (the 1st row in Table 3 is the average of data presented in Fig. 2) are shown. The points in Fig. 2 are average values for each run normally based on 30 droplets. The difference in the initial distance between drops can be due to changes in the room temperature, deviations in viscosity of dispersed phase, fluctuations in flow rate output of syringe pumps and some memory effects of the system. It is seen that despite a large scatter in the results the general trend in increasing of percentage of non-coalesced drops with increase of distance is obvious. We tried to keep the distance between drops in various systems close to each other, but if

Table 3 – Coalescence rate of surfactant-free and surfactant-laden drops in the straight output channel.

Surfactant	C, mM	Q_c, μL/min	Q_d, μL/min	L, mm	D, μm	Δ, μm	Non-coalesced, %
No		10	14	3.4	289 ± 5	45 ± 9	67 ± 8
C_{12}TAB[a]	150	6	10	3.0	285 ± 4	61 ± 6	21 ± 4
SDS	50	10	10	3.0	264 ± 4	53 ± 11	49 ± 6
Triton X-100	50	10	7	5.0	204 ± 2	83 ± 3	51 ± 12
Span 80	25	7	10	1.9	290 ± 5	35 ± 8	26 ± 3
Span 80	25	8	10	3.4	279 ± 7	58 ± 5	34 ± 8
Span 80	25	10	10	5.6	270 ± 5	84 ± 4	53 ± 10

[a] Data from Kovalchuk et al. (2017).

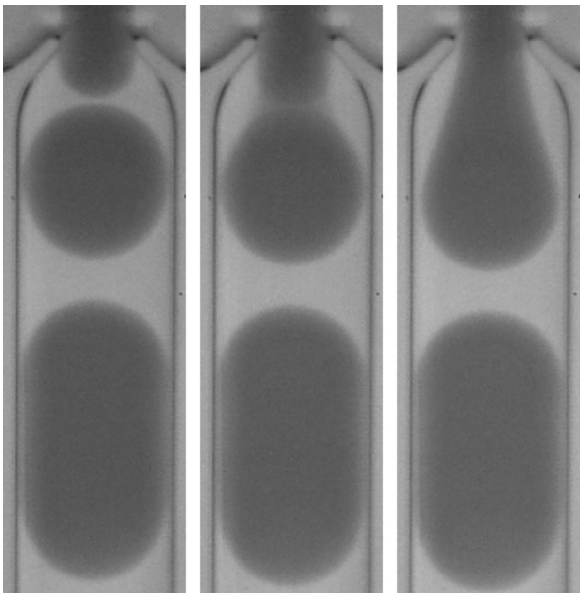

Fig. 3 – Drop coalescence at junction. Time between frames 1 ms.

this was not possible the observation length was increased proportionally to the distance between drops.

Results on drop coalescence including flow rates, Q_c and Q_d, surfactant concentration, C, the drop diameter in the plane of observation, D, the average surface to surface distance between drops, Δ, and the observation length, L, are presented in Table 3. At $Q_d \leq 40$ μL/min and $2 < Q_d/Q_c \leq 10$ coalescence of two drops occurred at junction (Fig. 3) resulting in formation of rather monodisperse set of drops of larger size.

By keeping flow rates unchanged, addition of surfactant results in a decrease of the drop size and in corresponding increase of the surface to surface distance. Analysis of results on the drop size obtained in this study shows that at drop production in dripping regime (Kovalchuk et al., 2017), which is used in this study the decrease is rather slow, with $D \sim \sigma^{\beta}$, where $0.1 < \beta < 0.2$. This is in good agreement with analysis presented in Cubaud and Mason (2008), which resulted in $\beta = 0.17$. The anionic surfactant SDS decreases the interfacial tension by approximately 3 times when compared with surfactant-free system (Table 2) and therefore demonstrates the closest values of D and Δ to surfactant-free system. Despite the larger surface to surface distance the SDS-laden drops demonstrate considerably larger rate of coalescence as compared to surfactant-free system. Therefore it can be concluded that in agreement with Kovalchuk et al. (2017) ionic surfactants do not stabilise, but destabilise drops and facilitate coalescence.

Interfacial tension in the system with the non-ionic surfactant Triton X-100 is only 3 mN/m, i.e. nearly 10 times smaller than in surfactant-free case affecting both, drop size and regime transition. At $Q_c = Q_d = 10$ μL/min drops formation occurs in jetting regime (Kovalchuk et al., 2017) with distance between drops being around 360 μm, i.e. 9 times larger than for surfactant-free system, therefore no coalescence was observed over the channel length. The minimum possible distance between drops laden by Triton X-100 was around 83 μm (Table 3). Considering large difference in the distance between drops between surfactant-laden and surfactant-free system and large experimental error for drops of Triton X-100 solution it is impossible to conclude whether there is destabilising effect, but certainly there is no noticeable stabilisation of drop by this non-ionic surfactant.

For Span 80 dissolved in the oil phase three flow rates of continuous phase are included in Table 3 confirming that in the presence of surfactant, similar to surfactant-free drops, an increase in the distance between drops results in a decrease of coalescence rate. At $Q_c = 7$ μL/min the initial distance between drops is smaller than between surfactant-free drops, whereas at $Q_c = 10$ μL/min it is nearly twice as large. Nevertheless the percentage of non-coalesced drops is smaller than that of surfactant-free drops in all three cases. This shows that this non-ionic surfactant also has destabilising rather than stabilising effect of formed drops. Note, the largest distance between drops in the presence of Span 80 is close to the distance between Triton X-100 laden drops and the percentages of non-coalesced drops are also close to each other. Therefore it can be assumed that the coalescence rate for drops of this surfactant solution will be higher than surfactant-free drops at similar surface to surface distance.

For SDS and Triton X-100 concentration of 50 mM was chosen to be sure that on time scale of drop formation surfactant reaches the equilibrium adsorption. This was proven by measuring dynamic surface tension of corresponding solutions. Concentration of Span 80 in silicone was limited by its solubility and was only 25 mM. As surfactant was dissolved in oil it was impossible to estimate dynamic surface tension for this solution (surfactant is active on the interface with aqueous phase, but not with air). Therefore, despite the low value of equilibrium interfacial tension, ~1 mN/m, the real interfacial tension at the moment of drop formation and the completeness of adsorption layer is unknown. From comparison of drop sizes and regimes with those of SDS and Triton X-100 solutions at the same flow rates, it can be concluded that interfacial tension between oil and aqueous phase is close to that of SDS and therefore the interface is not completely covered by surfactant. The time of drop formation is around 50 ms at flow rates shown in Table 3, whereas time of drop travelling over the observation length is ~400 ms at $Q_c = 7$ μL/min and ~700 ms at $Q_c = 10$ μL/min. Therefore in both cases the adsorption layers should be close to completeness at the end of observation length.

3.2. *Velocity fields due to coalescence*

When a drop moves along the channel its velocity is larger than superficial liquid velocity found as $V_s = (Q_d + 2Q_c)/S$, where S is the cross-sectional area of output channel. The relative velocity increases with a decrease of the drop size. For surfactant-free drops of 289 μm (Table 3) the superficial velocity at $Q_c = 10$ μL/min, $Q_d = 14$ μL/min, $V_s = 8.54$ mm/s, velocity at the tip of the drop of dispersed phase found from image processing $V_d = 9.0$ mm/s and the ratio of drop velocity to superficial liquid velocity $V_d/V_s = 1.05$, whereas for drop of Triton X-100 with $D = 204$ μm this ratio increases to 1.27. These values of V_d/V_s are in line with the drift-flux model predicting $1.1 < V_d/V_c < 1.3$ for bubbly flows in liquid (Clark and Flemmer, 1985) as well as with results presented in Jakiela et al. (2011), where it was also found that at the small viscosity contrast ratio between dispersed and continuous phase, what is the case of the present study, V_d/V_s is independent of capillary number. There is no noticeable recirculation due to interaction with the channel walls for drops having a circular shape in the plane of observation. Recirculation was observed only for plugs with length considerably higher than the channel width as shown in Fig. 4 which is in agreement with (Sarrazin et al., 2006; Seemann et al., 2012). Pirbodaghi et al. (2015) found well defined recirculatory flow in drops with size noticeably smaller than the channel width, but at drop velocity 55 mm/s which is considerably higher than velocities in the present study. Recirculatory flow was also found in slugs of continuous phase dividing air bubbles in mm-size tubes, where it was initiated by the direct contact of continuous phase with the tube walls (Tsoligkas et al., 2007).

Changes in flow fields inside the surfactant-free drops during their merging are shown in Fig. 5. When drops approach each other they move as a doublet for some time (<1 ms). The flow field in each drop at this stage reflects its translational motion as shown in Fig. 5, $t = 0$. There is no noticeable recirculation inside the drops in the plane of observation. In the contact zone the drops form a film with diameter around 70–80 μm.

At the instant of coalescence the thin oil film separating the drops breaks and the diameter of neck connecting the merging drops increases due to excessive capillary pressure in the neck. Therefore liquid from both drops moves towards the neck causing recirculation (Fig. 5). In Fig. 5 the velocity of translational motion is subtracted from the velocity fields at $t > 0$. The strongest internal convection develops at the beginning of the merging, when neck diameter increases very quickly as shown in Fig. 6, curve 1 (red points). For the particular case presented in Figs. 5 and 6 curve 1 the neck kinetics slow down around 0.3 ms. Reliable data on the velocity distribution were obtained only for $t > 0.3$ ms (Fig. 7), which show that the maximum convective velocity is more than one order of magnitude larger than the velocity of the drops in the channel. The velocity of recirculation still remains noticeably higher than the velocity of translational motion at $t = 5$ ms (Fig. 5). Note, comparison of the neck kinetics for drops with and without nanoparticles has shown that the presence of nanoparticles does not influence the drop merging.

It is obvious from Fig. 5 that recirculation due to merging of similar drops is limited to the individual drops and does not mix their contents. However indirectly such recirculation facil-

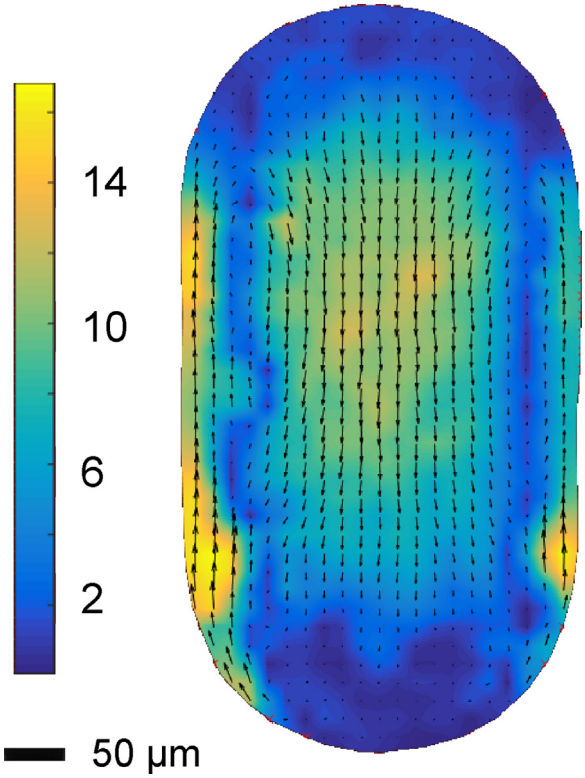

Fig. 4 – Recirculation inside the plug of surfactant free aqueous phase formed in flow-focusing device at $Q_c = 10$ μL/min, $Q_d = 50$ μL/min. Plug length is 648 μm. Velocity on colour scale is presented in mm/s.

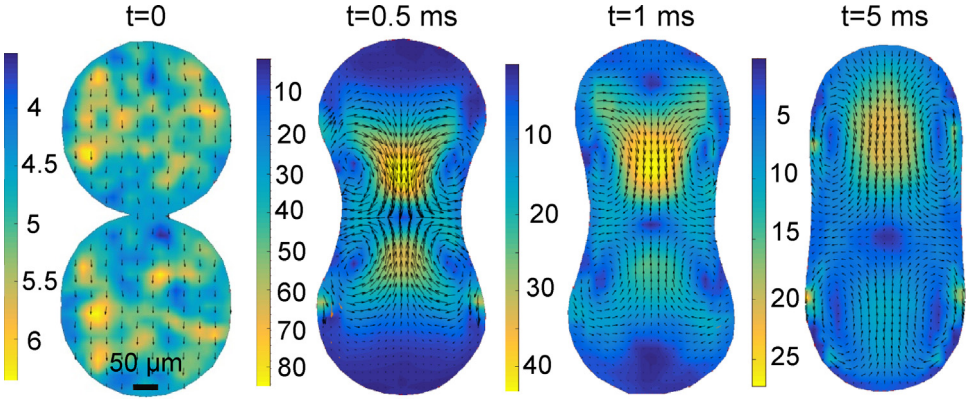

Fig. 5 – Flow fields resulting from the merging of two surfactant-free drops at $Q_c = 3$ μL/min, $Q_d = 10$ μL/min. Drop size $D = 372$ μm. The average velocity of drops translational motion before coalescence if subtracted from the flow fields at >0. Velocity on colour scales is presented in mm/s.

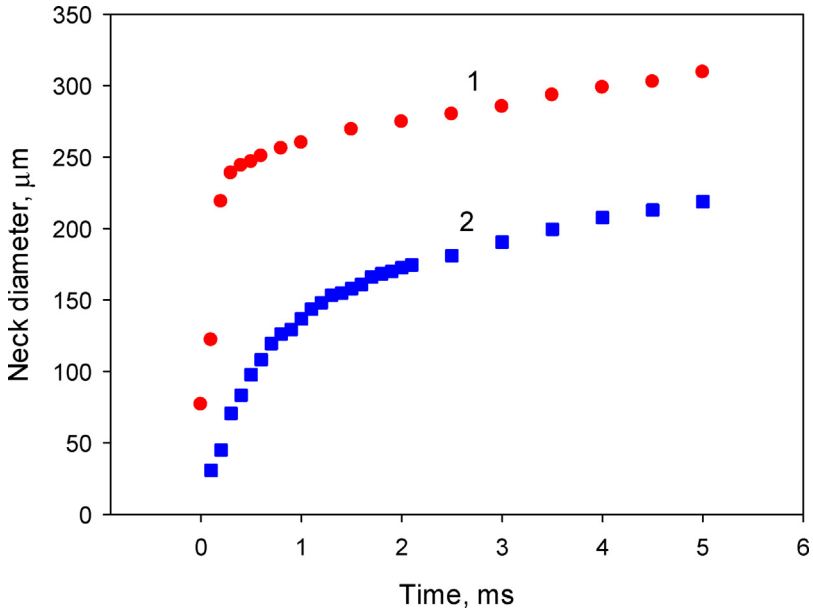

Fig. 6 – Kinetics of neck during the drop merging: (1) surfactant-free system, $Q_c = 3$ μL/min, $Q_d = 10$ μL/min; 50 mM Triton X-100 in dispersed phase, $Q_c = 10$ μL/min, $Q_d = 7$ μL/min.

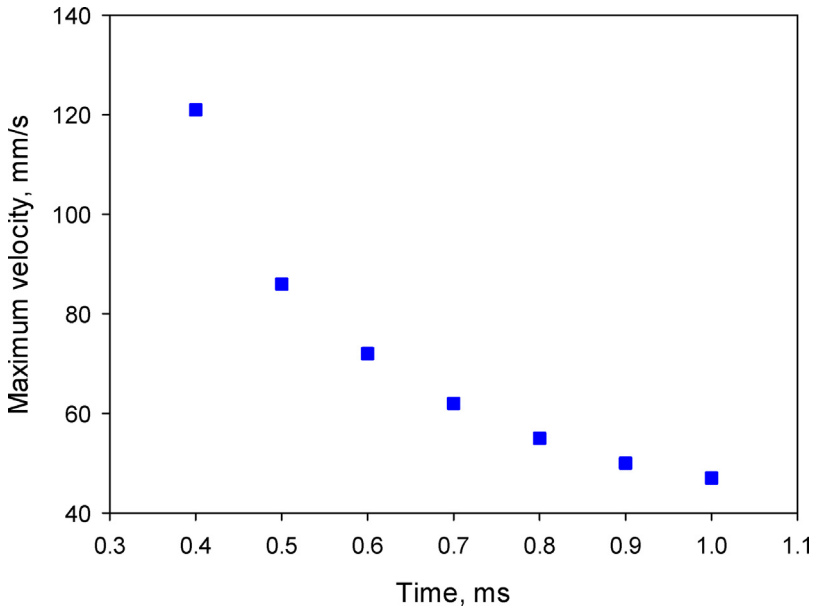

Fig. 7 – Maximum velocity inside the merging surfactant-free drops at $Q_c = 3$ μL/min, $Q_d = 10$ μL/min.

itates mass transfer between drops, because it bring solutes from the bulk of each drop to the symmetry plane increasing in this way concentration gradients. With time the recirculation in the first drop becomes considerably less intensive than in the second drop because the interaction with the channel wall decelerates the former and accelerates the latter.

The driving force of the drop merging is the difference in the capillary pressure between the drops and connecting bridge. As capillary pressure $P_c = 2\sigma/D$ is inversely proportional to the drop size, smaller drops merge faster and recirculation inside of them is more intensive what is confirmed by Fig. 8 and Table 4. Addition of surfactant results in a decrease of interfacial tension and therefore in slower neck kinetics (compare curves 1 and 2 (blue points) in Fig. 6) and slower recirculation (Table 4).

Analysis of the data of Table 4 shows that the effect of size is more pronounced for the large drops. For example the same maximum velocity, 45 mm/s, after 1 ms of merging was observed for surfactant-free drops with $D = 372$ μm (the 1st line in Table 4) and the drops of C_{12}TAB solutions with $D = 289$ mm (4th line) despite more than 2 times larger capillary pressure in the former case. At the same time for smaller drops the maximum velocity is nearly proportional to the capillary pressure: for results presented in the two last lines of Table 4 the ratio of maximum velocities is 2 and the ratio of capillary pressures is 2.2. This effect can be explained as follows. When drops merge and neck diameter increases the continuous phase is expelled from the neck region to the space below and above the merging drops. When drops are large the film between the drop and the channel wall is thin and has large hydrodynamic resistance. It slows down the expelling the continuous phase and therefore slows down the merging as compared to the drops of smaller size. This size dependence is also seen in Fig. 8. The difference in the recirculation rate between the lower and the upper drop is larger for the larger drops because of the stronger friction effect.

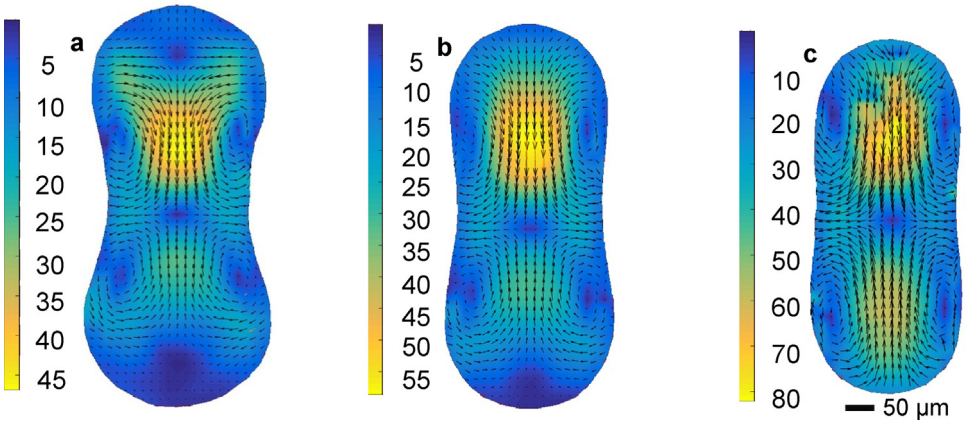

Fig. 8 – Dependence of the recirculation inside the merging surfactant-free drops on their size: (a) Q_c = 3 μL/min, Q_d = 10 μL/min, D = 372 μm; (b) Q_c = 6 μL/min, Q_d = 20 μL/min, D = 348 μm; (c) Q_c = 10 μL/min, Q_d = 30 μL/min, D = 326 μm; t = 1 ms. The average velocity of drops translational motion before coalescence if subtracted from the flow fields. Velocity on colour scales is presented in mm/s.

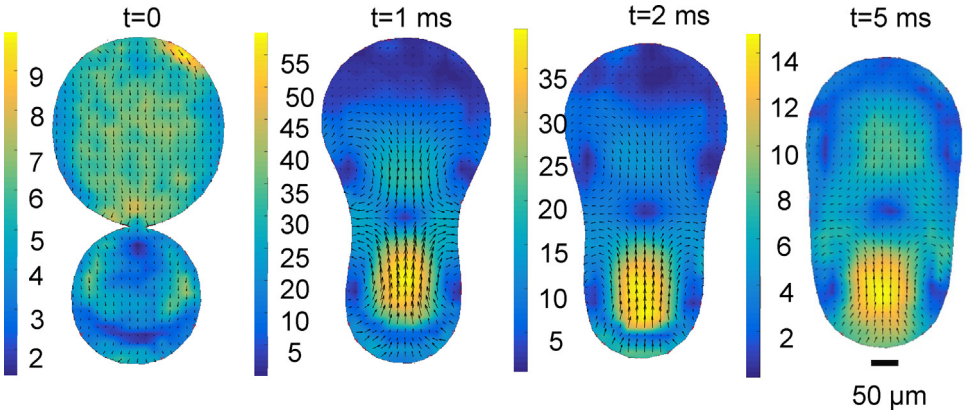

Fig. 9 – Coalescence of drops of C_{12}TAB solution of different sizes: 267 μm and 369 μm. The average velocity of translational motion is subtracted from the flow fields at >0. Velocity on colour scales is presented in mm/s.

Table 4 – Dependence of the intensity of recirculation inside the similar drops on their size and interfacial tension.

Surfactant	Q_c, μL/min	Q_d, μL/min	Ratio of drop and channel size	Interfacial tension, mN/m	Maximum velocity (after 1 ms), mm/s
No	3	10	0.95	30	45
No	6	20	0.89	30	55
No	10	30	0.84	30	80
C_{12}TAB	6	10	0.74	10	45
C_{12}TAB	10	10	0.66	10	50
C_{12}TAB	20	10	0.58	10	60
Triton X-100	10	6	0.52	4	30

Flow fields resulted from the coalescence of the drops of different size is shown in Fig. 9. In this case capillary pressure inside the drops is different resulting in the different intensity of convection inside the drops. Moreover in this case there is mass transfer between the drops: the small drop contents moves into the larger drop. The initial ratio of drop areas in the plane of observation was around 0.55 whereas after 5 ms the dividing plane corresponding to the zero vertical velocity moved in direction of the large drop and the area difference increased to 0.78. A similar mixing was observed for the drops of mm-size merging in unconfined geometry (Nowak et al., 2017).

4. Conclusions

Study on drop coalescence in a straight channel of a flow focusing microfluidic device has shown that in the confined geometry the presence of surfactant does not always stabilise the drops. Using ionic surfactant dissolved in the dispersed phase as well as non-ionic surfactant dissolved in dispersed or in continuous phase it was found that the drop coalescence rate was not smaller, but even larger for surfactant laden drops as compared with surfactant-free drops. The obtained results indicate that the destabilising effect of surfactant on drops in microchannel does not depend on the nature of surfactant or the phase where it is dissolved.

Ghost Particle Velocimetry allowed visualisation of the flow patterns inside merging drops without distortion of the flow field. This was possible by matching the refractive index of dispersed and continuous phase. Moreover, thanks to the use of nanoparticles at a low concentration as tracers, the flow field was not perturbed by their presence.

Drop merging was accompanied by strong recirculation inside the drops with maximum velocity of recirculation being more than 1 order of magnitude larger than the velocity of

translational motion of the drops. The rate of recirculation increased with the decrease of drop size, but decreased with the decrease of interfacial tension between continuous and dispersed phase. The effect of size was especially strong at drop sizes close to the channel width due to considerably thinner film of continuous phase separating dispersed phase from the channel wall, slower expelling of continuous phase surrounding growing neck between merging drops and therefore slower neck thickening.

For the drops of the similar size the recirculation occurred within each drop without any convective mixing between drops. For the drops of different size stronger recirculation was observed in the smaller drop and the content of the smaller drop was moved towards the larger drop.

Acknowledgements

This work is funded by the EPSRC Programme Grant "MEMPHIS – Multiscale Examination of Multiphase Physics in Flows" (EP/K003976/1). J. Chowdhury acknowledges the University of Birmingham for financial support of his summer research project. Z. Schofield acknowledges EPSRC Physical Sciences for Health CDT for provision of her studentship (EP/L016346/1).

References

Anon, 1963. Physical Properties of Glycerine and its Solutions. Glycerine Producers' Association, New York.

Axt, B., Hsieh, Y.F., Nalayanda, D., Wang, T.H., 2017. Impedance feedback control of microfluidic valves for reliable post processing combinatorial droplet injection. Biomed. Microdevices 19, 61.

Baret, J.C., 2012. Surfactants in droplet-based microfluidics. Lab Chip 12, 422–433.

Blanchette, F., 2010. Simulation of mixing within drops due to surface tension variations. Phys. Rev. Lett. 105, 074501.

Bremond, N., Bibette, J., 2012. Exploring emulsion science with microfluidics. Soft Matter 8, 10549–10559.

Bringer, M.R., Gerdts, C.J., Song, H., Tice, J.D., Ismagilov, R.F., 2004. Microfluidic systems for chemical kinetics that rely on chaotic mixing in droplets. Philos. Trans. R. Soc. Lond. A 362, 1087–1104.

Buzzaccaro, S., Secchi, E., Piazza, R., 2013. Ghost particle velocimetry: accurate 3D flow visualization using standard lab equipment. Phys. Rev. Lett. 111, 048101.

Casadevall i Solvas, X., Srisa-Art, M., deMello, A.J., Edel, J.B., 2010. Mapping of fluidic mixing in microdroplets with 1 μs time resolution using fluorescence lifetime imaging. Anal. Chem. 82, 3950–3956.

Chinaud, M., Voulgaropoulos, V., Angeli, P., 2016. Surfactant effects on the coalescence of a drop in a Hele-Shaw cell. Phys. Rev. E 94, 033101.

Clark, N.N., Flemmer, R.L., 1985. Predicting the holdup in two-phase bubble upflow and downflow using the Zuber and Findlay drift-flux model. AIChE J. 31, 500–503.

Cubaud, T., Mason, T.G., 2008. Capillary threads and viscous droplets in square microchannels. Phys. Fluids 20, 053302.

DeMello, A.J., 2006. Control and detection of chemical reactions in microfluidic systems. Nature 442, 394–402.

Frenz, L., El Harrak, A., Pauly, M., Bégin-Colin, S.B., Griffiths, A.D., Baret, J.C., 2008. Droplet-based microreactors for the synthesis of magnetic iron oxide nanoparticles. Angew. Chem. Int. Ed. 47, 6817–6820.

Gu, H., Duits, M.H.G., Mugele, F., 2011. Droplets formation and merging in two-phase flow microfluidics. Int. J. Mol. Sci. 12, 2572–2597.

Hung, L.H., Choi, K.M., Tseng, W.Y., Tan, Y.C., Shea, K.J., Lee, A.P., 2006. Alternating droplet generation and controlled dynamic droplet fusion in microfluidic device for CdS nanoparticle synthesis. Lab Chip 6, 174–178.

Jakiela, S., Makulska, S., Korczyk, P.M., Garstecki, P., 2011. Speed of flow of individual droplets in microfluidic channels as a function of the capillary number, volume of droplets and contrast of viscosities. Lab Chip 11, 3603–3608.

Jin, B.J., Yoo, J.Y., 2012. Visualization of droplet merging in microchannels using micro-PIV. Exp. Fluids 52, 235–245.

Kovalchuk, N.M., Roumpea, E., Nowak, E., Chinaud, M., Angeli, P., Simmons, M.J.H., 2018. Effect of surfactant on emulsification in microchannels. Chem. Eng. Sci. 176, 139–152.

Lee, S., Kim, H., Won, D.J., Lee, J., Kim, J., 2016. On-demand, parallel droplet merging method with non-contact droplet pairing in droplet-based microfluidics. Microfluid. Nanofluid. 20, 1.

Martin, D.W., Blanchette, F., 2015. Simulations of surfactant effects on the dynamics of coalescing drops and bubbles. Phys. Fluids 27, 012103.

Martino, C., Vigolo, D., Casadevall i Solvas, X., Stavrakis, S., DeMello, A.J., 2016. Real-time PEGDA-based microgel generation and encapsulation in microdroplets. Adv. Mater. Technol. 1, 1600028.

Nowak, E., Xie, Z., Kovalchuk, N.M., Matar, O.K., Simmons, M.J.H., 2017. Bulk advection and interfacial flows in the binary coalescence of surfactant-laden and surfactant-free drops. Soft Matter 13, 4616–4628.

Nurdin, L., Venancio-Marques, A., Rudiuk, S., Morel, M., Baigl, D., 2016. High-throughput photocontrol of water drop generation, fusion, and mixing in a dual flow-focusing microfluidic device. C. R. Chim. 19, 199–206.

Pirbodaghi, T., Vigolo, D., Akbari, S., DeMello, A., 2015. Investigating the fluid dynamics of rapid processes within microfluidic devices using bright-field microscopy. Lab Chip 15, 2140–2144.

Rhee, M., Burns, M.A., 2008. Drop mixing in a microchannel for lab-on-a-chip platforms. Langmuir 24, 590–601.

Sarrazin, F., Loubiere, K., Prat, L., Gourdon, C., Bonometti, T., Magnaudet, J., 2006. Experimental and numerical study of droplets hydrodynamics in microchannels. AIChE J. 52, 4061–4070.

Sarrazin, F., Prat, L., Di Miceli, N., Cristobal, G., Link, D.R., Weitz, D.A., 2007. Mixing characterization inside microdroplets engineered on a microcoalescer. Chem. Eng. Sci. 62, 1042–1048.

Seemann, R., Brinkmann, M., Pfohl, T., Herminghaus, S., 2012. Droplet based microfluidics. Rep. Prog. Phys. 75, 016601.

Song, H., Tice, J.D., Ismagilov, R.F., 2003. A microfluidic system for controlling reaction networks in time. Angew. Chem. Int. Ed. 42, 768–772.

Stone, H.A., Stroock, A.D., Ajdari, A., 2004. Engineering flows in small devices: microfluidics toward a lab-on-a-chip. Annu. Rev. Fluid Mech. 36, 381–411.

Thielicke, W.W., Stamhuis, E.J., 2014. PIVlab – towards user-friendly, affordable and accurate Digital Particle Image Velocimetry in MATLAB. J. Open Res. Softw. 2, e30.

Tice, J.D., Song, H., Lyon, A.D., Ismagilov, R.F., 2003. Formation of droplets and mixing in multiphase microfluidics at low values of the Reynolds and the capillary numbers. Langmuir 19, 9127–9133.

Tsoligkas, A.N., Simmons, M.J.H., Wood, J., 2007. Influence of orientation upon the hydrodynamics of gas–liquid flow for square channels in monolith supports. Chem. Eng. Sci. 62, 4365–4378.

Whitesides, G.M., 2006. The origins and the future of microfluidics. Nature 442, 368–373.

Yeh, S.I., Fang, W.F., Sheen, H.J., Yang, J.T., 2013. Droplets coalescence and mixing with identical and distinct surface tension on a wettability gradient surface. Microfluid. Nanofluid. 14, 785–795.